THE UNIVERSITY OF WARWICK

N incorporation and associated localized vibrational modes in GaSb

J. Buckeridge,[1,*] D. O. Scanlon,[1,2] T. D. Veal,[3] M. J. Ashwin,[4] A. Walsh,[5] and C. R. A. Catlow[1]

[1]*University College London, Kathleen Lonsdale Materials Chemistry, Department of Chemistry, 20 Gordon Street, London WC1H 0AJ, United Kingdom*

[2]*Diamond Light Source Ltd., Diamond House, Harwell Science and Innovation Campus, Didcot, Oxfordshire OX11 0DE, United Kingdom*

[3]*Stephenson Institute for Renewable Energy, The University of Liverpool, Liverpool L69 7ZF, United Kingdom*

[4]*Department of Chemistry, University of Warwick, Coventry CV4 7AL, United Kingdom*

[5]*Centre for Sustainable Chemical Technologies and Department of Chemistry, University of Bath, Claverton Down, Bath BA2 7AY, United Kingdom*

We present results of electronic structure calculations on the N-related localized vibrational modes in the dilute nitride alloy GaSb$_{1-x}$N$_x$. By calculating the formation energies of various possible N incorporation modes in the alloy, we determine the most favorable N configurations, and we calculate their vibrational mode frequencies using density functional theory under the generalized gradient approximation to electron exchange and correlation, including the effects of the relativistic spin-orbit interactions. For a single N impurity, we find substitution on an Sb site, N$_{Sb}$, to be most favorable, and for a two-N-atom complex, we find the N-N split interstitial on an Sb site to be most favorable. For these defects, as well as, for comparison, defects comprising two N atoms on neighboring Sb sites and a N-Sb split interstitial on an Sb site, we find well-localized vibration modes (LVMs), which should be experimentally observable. The frequency of the triply degenerate LVM associated with N$_{Sb}$ is determined to be 427.6 cm^{-1}. Our results serve as a guide to future experimental studies to elucidate the incorporation of small concentrations of N in GaSb, which is known to lead to a reduction of the band gap and opens the possibility of using the material for long-wavelength applications.

I. INTRODUCTION

Dilute nitride alloys have been the focus of much experimental and theoretical study over the past two decades, both for their potential device applications and their unusual physical properties. When a small fraction of the As ions in GaAs or GaInAs are replaced with nitrogen, there is a considerable redshift in the band gap, with a 1% concentration of N leading to a band-gap reduction of approximately 150 meV [1,2], which opens up the possibility of long-wavelength telecommunications based on GaAs substrates [3,4], and of pushing the wavelength range of GaAs-based solar cells further into the infrared (IR) [5]. Associated with this decrease in band gap, however, is a substantial decrease in *n*-type carrier mobility, with mobilities of ∼200 cm^2 (V s)$^{-1}$, that are too low for many device applications at present, being typically found in samples [6–9]. Despite this restriction, world-record efficiency multijunction solar cells based on dilute nitrides have been produced [10].

Based on the band gaps of GaAs and GaN (1.5 and 3.4 eV, respectively) and Vegard's law, one would expect the band gap to increase, not decrease, as N is added to GaAs. To understand this unusual effect, there has been considerable theoretical and experimental work done to determine the nature of the N-induced electronic states in the material [11–21]. It has been found that the variation in band gap can be described well using a two-level band-anticrossing model [2,22–24], where N atoms substituting on As sites form resonant states above the conduction band edge (CBE), which push the conduction band down, resulting in the observed redshift. Clusters of N

atoms, occurring at random in the dilute alloy, have been proposed to introduce states close to or resonant with the CBE [19,25–27], which strongly modify the band dispersion and lead to observed variations in electron effective mass as the Fermi level is varied [28]. The reduction in mobility, known to occur in real samples, has been attributed to the scattering of carriers by these N cluster states close to the CBE, with resulting calculated mobilities and densities of states in close agreement with experiment [29–36]. Based on this mobility reduction, a method of experimentally probing the nature of the N-related electronic states, using a gated heterostructure device, has been proposed [37].

Although the incorporation of small concentrations of N in GaAs has been extensively studied, the effect in the related material GaSb is less well characterized. Samples with low N content have been successfully prepared using molecular beam epitaxy [38–41], and the band gap has been observed to reduce (from 0.8 eV) by 300 meV with a 1% N concentration [42–45], opening the possibility of using the material to replace cadmium mercury telluride in IR and thermal imaging applications in the 2–5 μm wavelength range and, when alloyed with In, the 8–14 μm range [46,47]. The reduction observed in GaSb is significantly larger than that observed in GaAs with a similar N content, indicating that the N-related electronic states may be different, or that N clustering may play a role in the band-gap reduction [48–51], although experimental probes of the nature of the N states remain elusive. Understanding N incorporation in GaSb and its similarities and differences with N incorporation in GaAs is therefore a priority, as it may help to resolve outstanding issues such as the role of clusters and interstitials in the dilute nitrides.

When N substitutes for an As ion in GaAs, due to the comparatively small size of N and the strength of the Ga—N

*j.buckeridge@ucl.ac.uk

bond, there is a triply degenerate localized vibrational mode (LVM) about the N atom (assuming the material is not strained [66]). LVM spectroscopy is a useful method of studying local bonding of impurities and complexes of impurities in semiconducting materials [52–54]. The N-related LVM has been studied extensively in GaAs, both experimentally, using Raman and IR spectroscopy [55–62], and theoretically, using density functional theory (DFT) [63–68], with good agreement between the two approaches. A similar approach may be taken to determine the nature of N-related defects in GaSb.

In this paper, we present results of DFT calculations on the vibrational modes associated with N incorporation in GaSb. We first determine the phonon distribution of pure GaSb, finding good agreement with experiment, indicating that our DFT approach is accurate. We then determine the formation energies of different N substitutional and interstitial defects in the neutral charge state, finding that the most favorable are, for incorporation of single N atoms, the substitutional N on an Sb site, N_{Sb}, and for incorporation of two N atoms forming a complex, the N-N split interstitial on an Sb site, $(N-N)_{Sb}$. We calculate the vibrational modes associated with these N-related defects, as well as, for comparison, the complex consisting of two N atoms on neighboring Sb sites, $N_{Sb} + N_{Sb}$, and the N-Sb split interstitial on an Sb site, $(N-Sb)_{Sb}$, which, although it has a relatively high formation energy according to our calculations, has been proposed to occur in significant concentrations in some samples, based on modeling of x-ray diffraction data [69]. For all the defects studied, we determine LVMs well separated from the top of the GaSb phonon bands, which should be possible to observe experimentally. Our results, therefore, serve as a guide to future experiments to determine the nature of the N impurity in dilute $GaSb_{1-x}N_x$ samples.

The rest of the paper is structured as follows: in Sec. II we present details of our calculations; in Sec. III we present our results; and in Sec. IV we summarize our findings.

II. CALCULATIONS

We have used DFT to determine the equilibrium structures and force constants of pure GaSb and GaSb containing N impurities. All our DFT calculations were carried out using the VASP code [70–73], utilizing the solids-corrected Perdew-Burke-Ernzerhof (PBEsol) generalized gradient approximation (GGA) exchange-correlation (XC) functional [74,75] with the projector augmented wave (PAW) method [76]. In addition to scalar-relativistic effects, spin-orbit interactions, which are known to have a significant effect on the valence-band dispersion in GaSb [77,78], have been explicitly included, as implemented in VASP. Ga $4d$ electrons have been included as valence electrons in the PAW pseudopotential.

To avoid the problem of Pulay stress, the two-atom primitive unit cell of GaSb was optimized at a series of different volumes with a 650 eV plane-wave cutoff and a $12 \times 12 \times 12$ Monkhorst-Pack [79] k-point mesh, which provided convergence in the total energy up to 10^{-5} eV. The resulting energy-volume data were fitted to the Murnaghan equation of state to derive the equilibrium lattice constant and bulk modulus.

Phonon frequencies of GaSb were determined using the frozen phonon approach, where the dynamical matrix is derived by displacing atoms from their equilibrium positions and calculating the resulting forces, thus giving the force constants. All force calculations were deemed converged when the change in total force on each ion per self-consistent field iteration was less than 10^{-4} eVÅ^{-1}. The phonon dispersions along the Δ, Σ, and Λ directions in the Brillouin zone were determined using a 64-atom, $2 \times 2 \times 2$ expansion of the cubic unit cell, as implemented in the post-processing program PHONOPY [80]. The splitting between the transverse optical (TO) and longitudinal optical (LO) modes was determined by a nonanalytical correction [81–83] using the experimental high-frequency dielectric constant, $\epsilon^\infty = 14.44$ [84], and Born effective charge, $Z^* = 1.9e$ [85], where e is the electronic charge. The elastic constants were determined from the stress-strain relation by performing six finite distortions of the lattice, as implemented in VASP.

The relaxed structures of the system containing N impurities were determined using 8- and 64-atom cubic supercells (9- and 65-atom supercells for calculations including interstitial N), using a plane-wave cutoff of 650 eV and a $4 \times 4 \times 4$ Monkhorst-Pack [79] k-point mesh. The supercells were relaxed at a series of different volumes, and the resulting energy versus volume data were fitted to the Murnaghan equation of state to determine the equilibrium structure. The calculations were deemed converged when the forces were less than 10^{-4} eVÅ^{-1}. The phonon frequencies were determined using the frozen phonon approach, with the calculated LVMs using the 8- and 64-atom supercells differing by less than 5% (apart from the configurations with two N atoms, where the difference rose to 8%), indicating that the frequencies are converged with respect to supercell size.

The formation energy of defect X, $E_f[X]$, assuming thermodynamic equilibrium, was determined (in the neutral charge state) from the equation:

$$E_f[X] = E_{tot}[X] - E_{tot}[bulk] - \sum_i n_i \mu_i, \qquad (1)$$

where $E_{tot}[bulk]$ is the total energy of the pure GaSb bulk supercell, $E_{tot}[X]$ is the total energy of the supercell containing X, n_i is the number of species i that is added to ($n_i > 0$) or removed from ($n_i < 0$) the supercell in forming X, and μ_i is the chemical potential of species i. The μ_i have been determined using the standard approach in supercell DFT calculations [86,87], which is as follows. We set the upper bound of μ_i (i-rich conditions) to be the energy of species i in its standard state, E_{SS}, and set the lower bound (i-poor conditions) to be $E_{SS} + \Delta H$, where ΔH is the enthalpy of formation of GaSb. We determine $\Delta H = -0.25$ eV, which is lower in magnitude than the experimental value of -0.43 eV. The discrepancy is probably due to using the GGA functional for electron XC. Using the experimental value, rather than the calculated value, however, would not alter the conclusions we draw from our results.

III. RESULTS

A. Bulk properties of GaSb

Our calculated structural and elastic properties of bulk zinc blende GaSb are presented in Table I, in comparison with experiment. The agreement between the calculated lattice

TABLE I. Calculated lattice parameter a, bulk modulus B, and elastic constants C_{11}, C_{12}, and C_{44} of zinc blende GaSb, compared with experiment.

	This work	Experiment
a (Å)	6.118	6.082[a]
B (GPa)	51.07	56.35[b]
C_{11} (GPa)	846	908[c]
C_{12} (GPa)	393	413[c]
C_{44} (GPa)	417	445[c]

[a]Reference [88].
[b]Reference [89].
[c]Reference [90].

constant a and the low-temperature measured value of Sirota and Gololobov [88] is very good, with a discrepancy of 0.6%. Our calculated bulk modulus B and elastic constants C_{11}, C_{12}, and C_{44} are lower than experiment, by ∼9% for B when compared with the room-temperature measurement of McSkimin *et al.* [89], and by ∼6% for the elastic constants in comparison with the low-temperature measurements of Boyle and Sladek [90], but they are within the same level of accuracy as previous calculations at a similar level of theory [91–95].

The calculated phonon dispersion of bulk GaSb is shown in Fig. 1, compared with inelastic neutron diffraction measurements [99] and first-order [96] and second-order [98] Raman scattering measurements. The agreement between the calculated acoustic mode dispersion and experiment is excellent, with discrepancies of less than 1%, apart from the longitudinal acoustic (LA) mode at the X point and the transverse acoustic (TA) branch in the Λ direction, where the discrepancy in some cases rises to just under 5%. The calculated optical mode dispersion, however, is slightly (1–8 %) softer than experiment, particularly in the Σ and Λ directions. As the frequencies at the high symmetry points agree well with experiment (within ∼3%), the calculated softer dispersion may
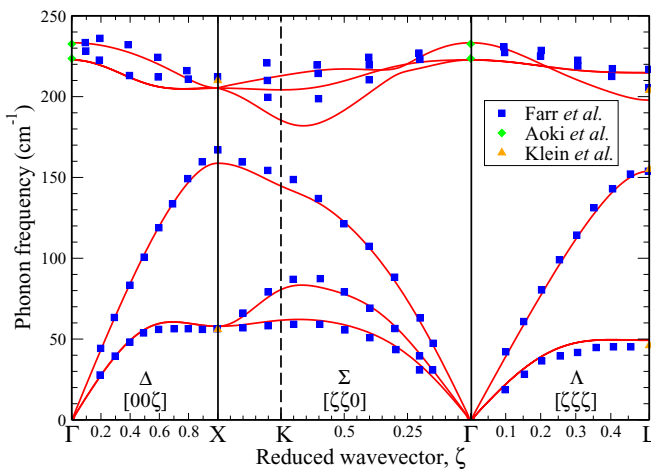

FIG. 1. (Color online) Calculated phonon dispersion curve for GaSb (solid red line) compared with measurements using first-order Raman scattering (green diamonds, Ref. [96]), second-order Raman scattering (orange triangles, Ref. [98]). and inelastic neutron scattering (blue squares, Ref. [99]) techniques.

TABLE II. Calculate values of the TO and LO phonon modes at the Γ point, ω_{TO} and ω_{LO}, compared with Raman scattering measurements.

	ω_{TO} (cm^{-1})	ω_{LO} (cm^{-1})
This work	222.7	233.3
Experiment[a]	223.6	232.6
Experiment[b]	226	235

[a]Reference [96].
[b]Reference [97].

be due to insufficient sampling of the Brillouin zone using our 64-atom supercell. We have calculated the transverse optical (TO) and longitudinal optical (LO) mode splitting at the Γ point using the nonanalytical correction approach [81–83], employing the experimentally determined values of ϵ^{∞} and Z^* (Refs. [84] and [85]; see Sec. II), to determine the TO and LO mode frequencies, ω_{TO} and ω_{LO}. Our results are in excellent agreement with the Raman measurements of Aoki *et al.* [96] and McGlinn *et al.* [97] (see Table II). The good agreement between our calculated phonon modes of GaSb and experiment indicates that our computational approach to determining the vibrational properties of the system gives accurate results. We note that our results also agree well with previous computational studies [82,100,101].

B. N-related defect formation energies

We next determined the formation energies of various N defects in GaSb in the neutral charge state, which are presented in Table III. We present the formation energies in Ga- and Sb-rich growth conditions, which refer approximately to the conditions in which samples may be prepared. We have considered incorporation of a single N atom on an Sb site, N_{Sb}, on a Ga site, N_{Ga}, on an interstitial tetrahedral site surrounded by Sb nearest-neighbors, N_i-Sb, and Ga nearest neighbors, N_i-Ga, and with an Sb on an Sb site as a split interstitial, $(N\text{-Sb})_{\text{Sb}}$. N_{Sb} is the most favorable configuration, being at least 1.05 eV lower in energy than the next most favorable, $(N\text{-Sb})_{\text{Sb}}$. We have therefore calculated the vibrational mode frequencies associated with this configuration. As $(N\text{-Sb})_{\text{Sb}}$ has been proposed to occur in significant concentrations in real samples [69], we have also calculated its associated mode frequencies, although we find

TABLE III. Calculated formation energies of N-related defects in the neutral charge state in Ga-rich and Sb-rich growth conditions. Energies are in eV.

	Ga-rich	Sb-rich
$E_f[\text{N}_{\text{Sb}}]$	1.20	1.45
$E_f[\text{N}_{\text{Ga}}]$	2.95	2.71
$E_f[\text{N}_i\text{-Sb}]$	3.82	3.82
$E_f[\text{N}_i\text{-Ga}]$	3.63	3.63
$E_f[(\text{N-Sb})_{\text{Sb}}]$	2.30	2.30
$E_f[\text{N}_{\text{Sb}} + \text{N}_{\text{Sb}}]$	2.39	2.88
$E_f[\text{N}_{\text{Sb}} + \text{N}_{\text{Ga}}]$	3.57	3.57
$E_f[(\text{N-N})_{\text{Sb}}]$	1.99	2.24

its formation to be unfavorable [102]. We find N_{Ga} to be highly unfavorable, with a formation energy at least 1.26 eV higher than N_{Sb}, and so we have not calculated the mode frequencies associated with it. We have considered the incorporation of two N atoms occurring on two nearest-neighbor Sb sites, $N_{Sb} + N_{Sb}$, on nearest-neighbor Ga and Sb sites, $N_{Sb} + N_{Ga}$, and as a N-N split interstitial on an Sb site, $(N-N)_{Sb}$. We find that the most favorable configuration is $(N-N)_{Sb}$, as forming this defect from two N atoms gains at least 0.21 eV per N atom. The split interstitial is similar in structure to an N_2 molecule, but with a larger bond length (1.38 Å *versus* the molecular bond length of 1.0977 Å [103]), related to the fact that some bond density delocalizes onto the surrounding Ga atoms. Incorporating two N atoms in the $N_{Sb} + N_{Sb}$ configuration gains ∼0.01 eV per N atom. As the formation energies of these two configurations are at least 0.69 eV more favorable than the other configuration considered, $N_{Sb} + N_{Ga}$, we have calculated the vibrational modes associated with them. Our results are presented below.

The N defects that include interstitial N can, in principle, accept up to three electrons. A more accurate picture of defect formation in the material should then include the different charge states associated with interstitial N, and determine the formation energy as a function of Fermi level [86,87,104,105]. To calculate the defect transition levels accurately, a higher level of theory than the GGA would need to be applied to treat electron exchange and correlation, such as hybrid-DFT, where a fraction of Hartree-Fock exchange is included explicitly [106–110]. Such a study is currently underway and the results will be reported elsewhere. The aim of the current study is to predict vibrational signatures of N-related defects, which may be probed experimentally using Raman or IR spectroscopy techniques, for which knowledge of the most likely N configurations to occur is necessary. Calculating the formation energies of the different N configurations in the neutral charge state, using our current DFT approach, provides sufficient information as to which configurations are favorable, assuming that the defects are not ionized. We have included charge in our calculations, with a charge-compensating (jellium) background, for the defects including interstitial N purely as an estimate of its lattice expansion effect (see below); we have not reported the resulting energetics of charged defects as we do not expect that using the GGA will be sufficiently accurate.

C. Effect of defect formation on the lattice constant

To assess which of the defect models we have proposed shows the closest agreement with experiment, we have calculated the resulting lattice contraction/expansion when a N defect is formed, including the additional effect of charging the defect where applicable, finding that our predictions on the most favorable defects lead to lattice constants in good agreement with experiment. We note that, in our periodic supercell approach, we are determining the effect of a regular array of N defects, rather than a random distribution. Since the strain introduced by each N atom, however, is highly localized (see below), and the interaction between the N atoms is weak, we expect our model to be a good approximation to a random N distribution (for charged defects, which do interact strongly, we

expect our approximation to be less good, so that the calculated lattice expansions in those cases are estimates).

Forming the defect N_{Sb} in our 64-atom supercell corresponds to a N concentration $x = 0.03125$. We find that this leads to a reduction in lattice constant of 0.86%, in good agreement with previous calculations [44]. Our calculated lattice constant, $a = 6.066$ Å at $x = 0.03125$, is in excellent agreement with measurements using secondary ion mass spectrometry (SIMS) to determine the N content, and x-ray diffraction (XRD) to determine the corresponding lattice constant, performed by Ashwin *et al.* [69]. We find that the N_{Sb} defect introduces a local strain in the system, so that the surrounding Ga atoms shift from their ideal lattice positions toward the N atom, resulting in a Ga—N bond length of 2.073 Å, a significant reduction from the calculated Ga—Sb bond length in the bulk GaSb system of 2.649 Å, constituting a change in lattice site position of ∼21% (including the overall lattice contraction effect associated with the N_{Sb}). The next-nearest-neighbor Sb atoms shift by 3.4% off their ideal lattice sites toward the N atom, while the third nearest-neighbor Ga atoms move very slightly (less than 1%) from their ideal lattice sites, and atoms beyond this experience no significant movement, excluding the overall lattice contraction. The highly localized strain gives an explanation for the observed deviation from Vegard's law, without the need to propose the formation of $(N-Sb)_{Sb}$ [69], which we find to be energetically unfavorable. Indeed, we find that the formation of neutral $(N-Sb)_{Sb}$ in our supercell, corresponding to $x = 0.03125$, leads to a lattice expansion of 0.22%, which increases to 1.71% when the defect is triply negatively charged. Considering the close agreement with experiment of our calculated lattice contraction due to the formation of N_{Sb}, we conclude that $(N-Sb)_{Sb}$ should not occur in significant quantities, which is consistent with our calculated formation energies for the two N configurations (see Table III). We find that the formation of N_i-Sb (N_i-Ga) leads to a lattice expansion in our supercell of 0.23% (0.20%), rising to 1.91% (1.81%) when triply negatively charged, again indicating that such configurations are unlikely to occur in significant quantities, which also follows from our calculated formation energies. We note that the deviation from Vegard's law observed in GaSb when N is added is qualitatively different from that in GaAs; when N is added to GaAs, the lattice constant reduction is *greater* than that expected from Vegard's law. Our calculations show then that the strain introduced by N in GaSb is significantly more localized than that in GaAs.

Incorporating two N atoms in our supercell corresponds to $x = 0.0625$. We find that forming the configuration $N_{Sb} + N_{Sb}$ leads to a lattice contraction of 1.68%, approximately double the contraction corresponding to the formation of N_{Sb}, which is much higher than would be expected from the trend in lattice constant versus N concentration observed by Ashwin *et al.* [69], which, at $x = 0.0625$, would give a lattice contraction of ∼1.1%. According to our calculations, the configuration $(N-N)_{Sb}$, however, leads to a lattice contraction of 0.43% in the neutral state, and a lattice expansion of 1.17% when it is triply negatively charged. At $x = 0.0625$, we determine that having 50% of the N incorporated as N_{Sb} and 50% incorporated as $(N-N)_{Sb}$, assuming the split interstitials are not ionized, would result in a contraction of 1.08%, which

would agree with the experimentally observed trend [if the split interstitials are triply charged, having 80% of the N as N_{Sb} and 20% as $(N\text{-}N)_{Sb}$ would be required]. We therefore conclude that the configuration $(N\text{-}N)_{Sb}$ should occur in significant quantities as x is increased, which agrees well with our calculated low formation energy of that configuration (see Table III). We suggest that such incorporation may also play a role in the observed dependence of N concentration on growth temperature [40] when x is determined by first using XRD to measure the lattice constant, and then assuming Vegard's law to hold, interpolating between the lattice constants of GaSb and GaN. As the temperature increases, the N atoms will become more mobile, enabling, according to our calculations, the formation of $(N\text{-}N)_{Sb}$, which will lead to a violation of Vegard's law, and hence to a perceived decrease in N concentration, if x is determined under the assumption that Vegard's law holds. A full analysis of such a procedure would require the diffusion activation energy of N in GaSb to be determined, as well as that of Ga or Sb vacancies in order to mediate the diffusion, which is beyond the scope of the present study. Instead, we suggest that the formation of $(N\text{-}N)_{Sb}$ may also contribute to the concentration versus temperature trend observed in Ref. [40], along with the increased desorption of N at higher temperatures.

The driving force for the formation of $(N\text{-}N)_{Sb}$ in GaSb is in contrast to the case of GaAs, where it costs ∼0.3 eV per N atom for the defect to form [111]. It has been claimed that $(N\text{-}N)_{As}$ plays a significant role in GaAs at higher N concentrations [112], but this point is controversial given the success of electronic structure and transport models that neglect them [26–29,31–33,35–37]. As we find that they play an important role in $GaSb_{1-x}N_x$ at higher N concentrations, which may be because they are more sterically favored, we propose that further study of this material will shed light on the nature and effect of these defects in the dilute nitrides, and help to clarify their role in the well-studied $GaAs_{1-x}N_x$ system.

D. Localized vibrational modes

We now turn to the calculated vibrational modes associated with the configurations N_{Sb}, $N_{Sb} + N_{Sb}$, $(N\text{-}N)_{Sb}$, and $(N\text{-}Sb)_{Sb}$. For each configuration, we find well-separated LVMs that should be experimentally observable. Our results are summarized in Table IV. We determine a triply degenerate, IR-active, LVM at 427.6 cm^{-1} associated with N_{Sb}. We find that the mode weight on the N atom is 94.6%, and the mode weight on the surrounding Ga atoms is 5.1%, meaning that the weight on the rest of the surrounding atoms is negligible. Single N substitution on an As site in GaAs results in a LVM at

470 cm^{-1} [57], which has been modeled accurately, resulting in a LVM frequency of 465 cm^{-1} [63,66], using a similar theoretical approach to the one we employ in the present work. Substitution of As by C in GaAs has been experimentally determined to result in a LVM at 582 cm^{-1} [113], which decreases by 42 cm^{-1} to 540 cm^{-1} for the case of C in GaSb [114]. A similar trend would be expected for N substitution in the two materials, as C and N are relatively similar in mass when compared to As and Sb (C being lighter than N results in the observed higher LVM). We indeed do see a similar trend, as our calculated LVM for N_{Sb} in GaSb (427.6 cm^{-1}) is ∼37 cm^{-1} lower than the calculated value for N_{As} in GaAs (465 cm^{-1}) [63,66].

We next consider the nearest-neighbor pair, $N_{Sb} + N_{Sb}$. From our calculated formation energies, we find a weak driving force for the formation of this configuration, with the configuration $(N\text{-}N)_{Sb}$ being more favorable; nevertheless, we calculated the associated vibrational modes in order to demonstrate the predicted broadening of the LVM associated with the single substitutional N_{Sb} due to the presence of other N_{Sb} nearby. The configuration consists of a N atom at $(0,0,0)$ and another at $(a/2,a/2,0)$, which has a C_{2v} symmetry and six nondegenerate modes associated with it. We determine their frequencies to be 449.1, 445.9, 428.0, 415.4, 339.7, and 324.2 cm^{-1}, and we show the associated N motion in Fig. 2. The vibrational modes that consist of N motion in the plane formed by the two N atoms and the shared nearest-neighbor Ga [Figs. 2(c)–2(f)] have slightly "crooked" N displacements; this effect can be attributed to the significant distortion of the shared Ga atom, which displaces by ∼30% from its ideal lattice site toward the two N atoms. Taking into account the reduction in the LVM frequency associated with single substitutional N on an anion site going from GaAs to GaSb, our results are consistent with those determined for N second-nearest neighbors in GaAs [65].

For the case of the $(N\text{-}N)_{Sb}$ configuration, we determine two doublet and two singlet modes. The associated motions are shown in Fig. 3. The lowest mode, at 250.0 cm^{-1}, is a doublet, consisting of the motion of one of the N atoms perpendicular to the N—N bond and to the plane containing its two nearest-neighbor Ga atoms, with the other N atom moving in phase in the same direction, but with a much lower amplitude [see Fig. 3(a)]. The frequency of this mode means that it lies close to the top of the GaSb phonon bands (at 233 cm^{-1}; see Fig. 1), which implies that it may form a resonance rather than a well-separated LVM, and it may be difficult to distinguish it from the host phonon modes. The next lowest mode, at 410.0 cm^{-1}, is a singlet (IR-active), consisting of in-phase motion of the two N atoms along their bond direction [see Fig. 3(b)], and it is the only mode we find within the $N_{Sb} + N_{Sb}$ broadened LVM range. We calculate another doublet at 608.7 cm^{-1}, with the associated atomic motions similar to those of the doublet at 250.0 cm^{-1}, except that the N atoms now move in opposite phases [i.e., a "wagging" mode; see Fig. 3(c)], and the greater amplitude of motion occurs in the plane containing the N atom and its two nearest-neighbor Ga atoms. Finally, we calculate a singlet at 941.8 cm^{-1}, corresponding to the Raman-active stretch mode [see Fig. 3(d)]. Our results are in close agreement with those calculated for a N-N split interstitial on an As site in GaAs [65],

TABLE IV. Calculated localized vibrational mode frequencies associated with different N configurations in GaSb.

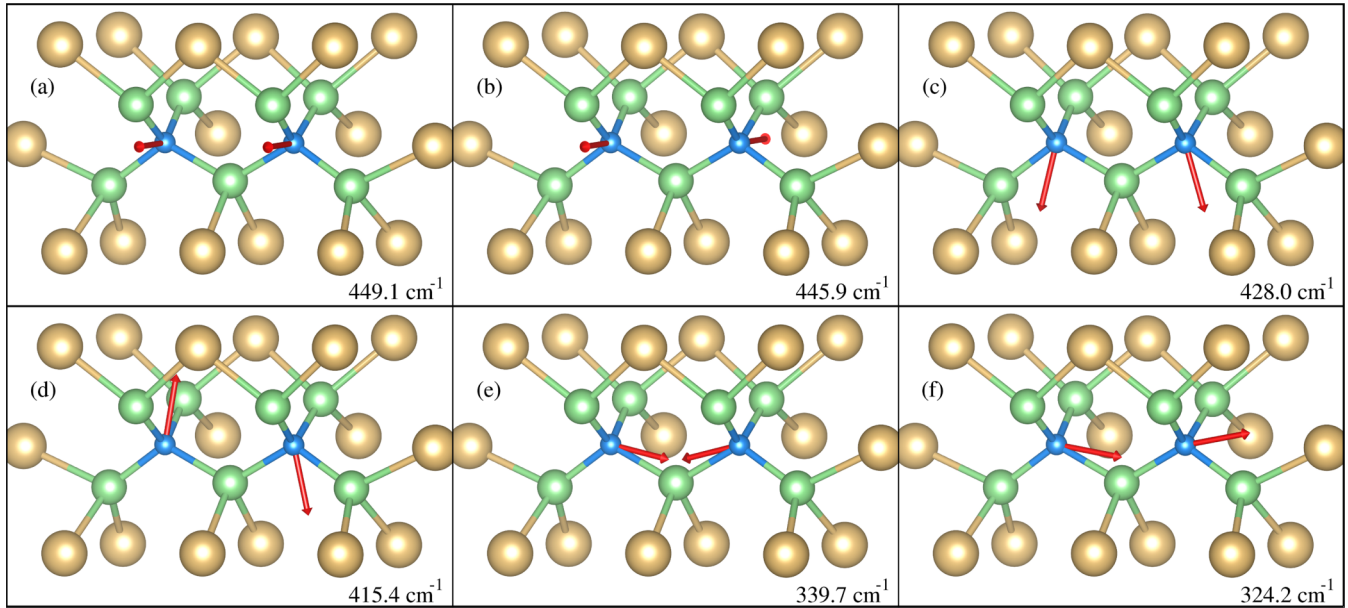| Configuration	Frequencies (cm^{-1})
N_{Sb}	427.6
$N_{Sb} + N_{Sb}$	324.2, 339.7, 415.4, 428.0, 445.9, 449.1
$(N\text{-}N)_{Sb}$	250.0, 410.0, 608.7, 941.8
$(N\text{-}Sb)_{Sb}$	236.6, 263.1, 627.5, 691.8

FIG. 2. (Color online) Vibrational modes associated with the $N_{Sb} + N_{Sb}$ configuration. Smaller dark gray (blue) spheres represent N atoms, light gray (green) spheres represent Ga atoms, and dark gray (gold) spheres represent Sb atoms. The arrows represent the mode displacements. For clarity, only some of the surrounding atoms are shown.

apart from the stretch mode, which we find to be lower by 139 cm^{-1}, consistent with our calculated N—N bond length of 1.38 Å being higher than that determined in GaAs, 1.36 Å [65], which in turn is related to the larger lattice constant of GaSb. We therefore see that the N-N split interstitial configuration in both GaAs and GaSb is quite similar, which indicates that

FIG. 3. (Color online) Vibrational modes associated with the (N-N)$_{Sb}$ configuration. Smaller dark gray (blue) spheres represent N atoms, light gray (green) spheres represent Ga atoms, and dark gray (gold) spheres represent Sb atoms. The arrows represent the mode displacements, with the magnitudes signifying the relative amplitudes. For clarity, only some of the surrounding atoms are shown.

the N—Ga bond strength in the two materials does not differ significantly. In both systems, the split interstitial stretch mode is lower than that of an N_2 molecule, 2358.57 cm^{-1} [103], which can be attributed to the greater bond length and lower bond strength than that of the molecule, resulting from the fact that some of the bonding density is delocalized onto surrounding atoms.
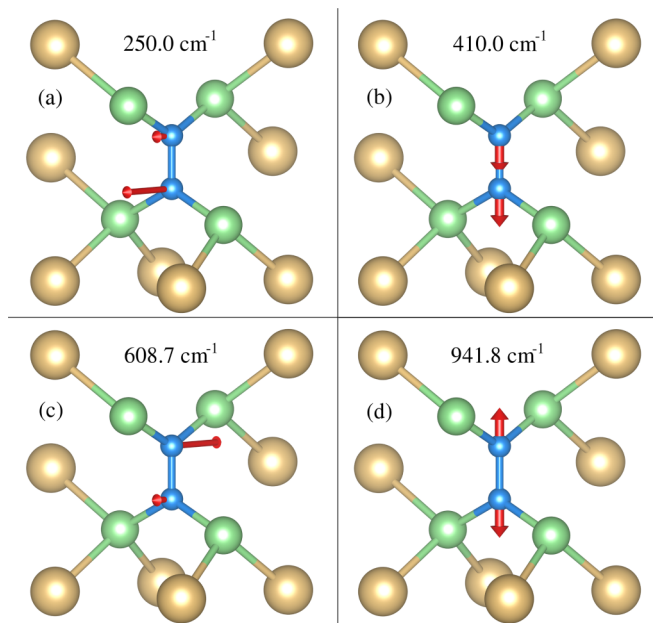
Finally, for the configuration (N-Sb)$_{Sb}$ we find four singlet LVMs (see Fig. 4). The lowest frequency LVM [236.6 cm^{-1}; see Fig. 4(a)] consists of a "wagging" motion of the Sb atom in the complex perpendicular to the N—Sb bond direction and parallel to the plane containing the Sb atom and its two nearest-neighbor Ga atoms, with the N atom moving in opposite phase but with an amplitude about six times smaller. This mode is very close to the top of the host GaSb phonon spectrum at 233 cm^{-1}, and so it will form a resonance. The next lowest frequency LVM [263.1 cm^{-1}; see Fig. 4(b)], which consists of the motion of the Sb atom along the N—Sb bond direction, with the N atom moving in phase but with an amplitude ~30 times smaller (not shown in the figure), is also close to the top of GaSb phonon bands, and so it may be difficult to distinguish it from the host phonon modes. The second highest frequency LVM [627.5 cm^{-1}; see Fig. 4(c)] is the IR- and Raman-active stretch mode, with the amplitude of the N atom approximately three times that of the Sb atom. The highest frequency LVM [691.8 cm^{-1}; see Fig. 4(d)] consists of N "wagging" motion perpendicular to the bond with the Sb atom forming the N—Sb complex and parallel to the plane containing the N atom and its two nearest-neighbor Ga atoms. The motions associated with the LVMs are similar to those determined for a N-As split interstitial on an As site in GaAs [65], but there are significant differences in the frequencies of the modes involving Sb motion, as would be expected. Indeed, the mode consisting of N motion alone, at 691.8 cm^{-1}, is practically identical to the corresponding mode
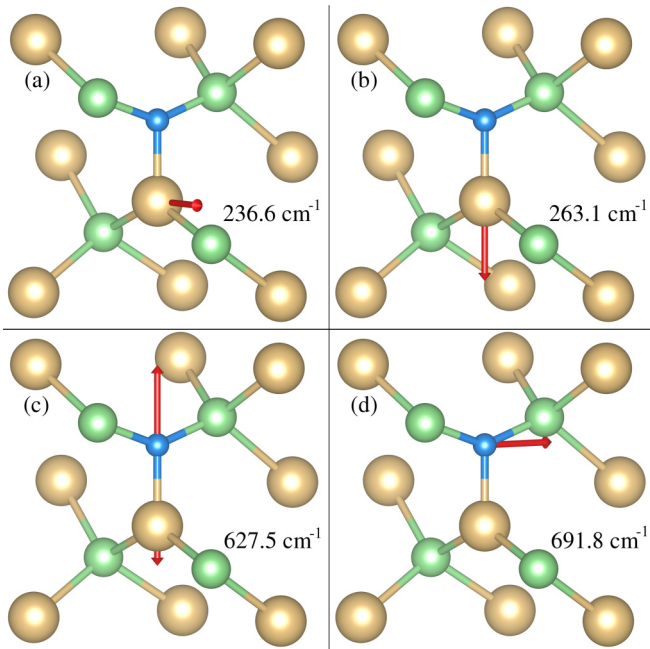
FIG. 4. (Color online) Vibrational modes associated with the (N-Sb)$_{Sb}$ configuration. Smaller dark gray (blue) spheres represent N atoms, light gray (green) spheres represent Ga atoms, and dark gray (gold) spheres represent Sb atoms. The arrows represent the mode displacements, with the magnitudes signifying the relative amplitudes. For clarity, only some of the surrounding atoms are shown.

in GaAs, 693 cm^{-1} [65]. The stretch mode, at 627.5 cm^{-1}, is significantly lower than the corresponding mode in GaAs, at 734 cm^{-1}, which is due to a combination of the higher mass of Sb in comparison with As and the greater bond length (2.02 Å for the N-Sb split interstitial in GaSb, compared with 1.78 Å [65] for the N-As split interstitial in GaAs). The effect is large enough to change the order of the modes, as the stretch mode is the highest frequency mode for the N-As split interstitial in GaAs. The corresponding modes to those consisting of mainly Sb motion, at 236.6 and 263.1 cm^{-1},

which would consist of mainly As motion, are not discussed in Ref. [65], indicating that they form resonances within the GaAs phonon bands, not LVMs. Although some of the calculated mode frequencies are close to those calculated for the (N-N)$_{Sb}$ configuration, there is a large enough difference between the ranges of the LVMs that their presence may be differentiated experimentally.

IV. SUMMARY AND CONCLUSIONS

We have studied the incorporation of N in GaSb using DFT. We find that the most stable configuration for single N incorporation is on an Sb site, N$_{Sb}$, while for two nearest-neighbor N atoms we find that the N$_{Sb}$ + N$_{Sb}$ and (N-N)$_{Sb}$ configurations are favored. For these configurations, and the (N-Sb)$_{Sb}$ configuration which has been previously proposed to occur in significant concentrations, we have calculated the associated vibrational mode frequencies, finding well-localized modes for all configurations studied, which should be experimentally observable. Our results serve as a guide to experimental investigations of N incorporation in GaSb, the nature of which is not well understood, using LVM spectroscopy.

[1] M. Weyers, M. Sato, and H. Ando, Jpn. J. Appl. Phys. **31**, L853 (1992).

[2] W. Shan, W. Walukiewicz, J. W. Ager, III, E. E. Haller, J. F. Geisz, D. J. Friedman, J. M. Olson, and S. R. Kurtz, Phys. Rev. Lett. **82**, 1221 (1999).

[3] H. Riechert, A. Ramakrishnan, and G. Steinle, Semicond. Sci. Technol. **17**, 892 (2002).

[4] J. S. Harris, Semicond. Sci. Technol. **17**, 880 (2002).

[5] J. F. Geisz and D. J. Friedman, Semicond. Sci. Technol. **17**, 769 (2002).

[6] D. L. Young, J. F. Geisz, and T. J. Coutts, Appl. Phys. Lett. **82**, 1236 (2003).

[7] R. Mouillet, L.-A. de Vaulchier, E. Deleporte, Y. Guldner, L. Travers, and J.-C. Harmand, Solid State Commun. **126**, 333 (2003).

[8] D. Fowler, O. Makarovsky, A. Patanè, L. Eaves, L. Geelhaar, and H. Riechert, Phys. Rev. B **69**, 153305 (2004).

[9] A. J. Ptak, S. W. Johnston, S. Kurtz, D. J. Friedman, and W. K. Metzger, J. Cryst. Growth **251**, 392 (2003).

[10] R. Jones-Albertus, E. Becker, R. Bergner, T. Bilir, D. Derkacs, O. Fidaner, D. Jory, T. Liu, E. Lucow, P. Misra, E. Pickett, F. Suarez, A. Sukiasyan, T. Sun, L. Zhang, V. Sabnis, M. Wiemer, and H. Yuen, Materials Research Society Proceedings Vol. 1538 (MRS, Pittsburgh, 2013), pp. 161–166.

[11] J. Endicott, A. Patanè, J. Ibáñez, L. Eaves, M. Bissiri, M. Hopkinson, R. Airey, and G. Hill, Phys. Rev. Lett. **91**, 126802 (2003).

[12] T. Dannecker, Y. Jin, H. Cheng, C. F. Gorman, J. Buckeridge, C. Uher, S. Fahy, C. Kurdak, and R. S. Goldman, Phys. Rev. B **82**, 125203 (2010).

[13] P. J. Klar, H. Grüning, W. Heimbrodt, J. Koch, F. Höhnsdorf, W. Stolz, P. M. A. Vicente, and J. Camassel, Appl. Phys. Lett. **76**, 3439 (2000).

[14] J. D. Perkins, A. Mascarenhas, Y. Zhang, J. F. Geisz, D. J. Friedman, J. M. Olson, and S. R. Kurtz, Phys. Rev. Lett. **82**, 3312 (1999).

[15] J. Wu, K. Yu, and W. Walukiewicz, IEE Proc.: Optoelectron. **151**, 460 (2004).

[16] L. Bellaiche, S.-H. Wei, and A. Zunger, Phys. Rev. B **54**, 17568 (1996).

[17] P. R. C. Kent and A. Zunger, Phys. Rev. B **64**, 115208 (2001).

[18] P. R. C. Kent, L. Bellaiche, and A. Zunger, Semicond. Sci. Technol. **17**, 851 (2002).

[19] E. P. O'Reilly, A. Lindsay, S. Tomić, and M. Kamal-Saadi, Semicond. Sci. Technol. **17**, 870 (2002).

[20] J. W. Ager, III and W. Walukiewicz, Semicond. Sci. Technol. **17**, 741 (2002).

[21] E. P. O'Reilly, A. Lindsay, P. J. Klar, A. Polimeni, and M. Capizzi, Semicond. Sci. Technol. **24**, 033001 (2009).

[22] H. P. Hjalmarson, P. Vogl, D. J. Wolford, and J. D. Dow, Phys. Rev. Lett. **44**, 810 (1980).

[23] X. Liu, M. Pistol, L. Samuelson, S. Schwetlick, and W. Seifert, Appl. Phys. Lett. **56**, 1451 (1990).

[24] M. Seifikar, E. P. O'Reilly, and S. Fahy, Phys. Status Solidi B **248**, 1176 (2011).

[25] F. Masia, G. Pettinari, A. Polimeni, M. Felici, A. Miriametro, M. Capizzi, A. Lindsay, S. B. Healy, E. P. O'Reilly, A. Cristofoli, G. Bais, M. Piccin, S. Rubini, F. Martelli, A. Franciosi, P. J. Klar, K. Volz, and W. Stolz, Phys. Rev. B **73**, 073201 (2006).

[26] A. Lindsay and E. P. O'Reilly, Solid State Commun. **118**, 313 (2001).

[27] A. Lindsay and E. P. O'Reilly, Physica E **21**, 901 (2004).

[28] A. Lindsay and E. P. O'Reilly, Phys. Rev. Lett. **93**, 196402 (2004).

[29] S. Fahy and E. P. O'Reilly, Appl. Phys. Lett. **83**, 3731 (2003).

[30] O. F. Sankey, J. D. Dow, and K. Hess, Appl. Phys. Lett. **41**, 664 (1982).

[31] S. Fahy, A. Lindsay, and E. P. O'Reilly, IEEE Proc.: Optoelectron. **151**, 352 (2004).

[32] S. Fahy, A. Lindsay, H. Ouerdane, and E. P. O'Reilly, Phys. Rev. B **74**, 035203 (2006).

[33] M. P. Vaughan and B. K. Ridley, Phys. Rev. B **75**, 195205 (2007).

[34] I. Bosa, D. McPeake, and S. Fahy, Phys. Rev. B **78**, 245206 (2008).

[35] M. Seifikar, E. P. O'Reilly, and S. Fahy, Phys. Rev. B **84**, 165216 (2011).

[36] M. P. Vaughan, S. Fahy, E. P. O'Reilly, L. Ivanova, H. Eisele, and M. Dähne, Phys. Status Solidi B **248**, 1167 (2011).

[37] J. Buckeridge and S. Fahy, Phys. Rev. B **84**, 144120 (2011).

[38] L. Buckle, B. R. Bennett, S. Jollands, T. D. Veal, N. R. Wilson, B. N. Murdin, C. F. McConville, and T. Ashley, J. Cryst. Growth **278**, 188 (2005).

[39] P. H. Jefferson, L. Buckle, B. R. Bennett, T. D. Veal, D. Walker, N. R. Wilson, L. F. J. Piper, P. A. Thomas, T. Ashley, and C. F. McConville, J. Cryst. Growth **304**, 338 (2007).

[40] M. J. Ashwin, T. D. Veal, J. J. Bomphrey, I. R. Dunn, D. Walker, P. A. Thomas, and T. S. Jones, AIP Adv. **1**, 032159 (2011).

[41] M. J. Ashwin, D. Walker, P. A. Thomas, T. S. Jones, and T. D. Veal, J. Appl. Phys. **113**, 033502 (2013).

[42] T. D. Veal, L. F. J. Piper, S. Jollands, B. R. Bennett, P. H. Jefferson, P. A. Thomas, C. F. McConville, B. N. Murdin,

L. Buckle, G. W. Smith, and T. Ashley, Appl. Phys. Lett. **87**, 132101 (2005).

[43] P. H. Jefferson, T. D. Veal, L. F. J. Piper, B. R. Bennett, C. F. McConville, B. N. Murdin, L. Buckle, G. W. Smith, and T. Ashley, Appl. Phys. Lett. **89**, 111921 (2006).

[44] A. Belabbes, M. Ferhat, and A. Zaoui, Appl. Phys. Lett. **88**, 152109 (2006).

[45] D. Wang, S. P. Svensson, L. Shterengas, G. Belenky, C. S. Kim, I. Vurgaftman, and J. R. Meyer, J. Appl. Phys. **105**, 014904 (2009).

[46] A. Rogalski, J. Antoszewski, and L. Faraone, J. Appl. Phys. **105**, 091101 (2009).

[47] T. Ashley, L. Buckle, G. W. Smith, B. N. Murdin, P. H. Jefferson, L. F. J. Piper, T. D. Veal, and C. F. McConville, Proc. SPIE **6206**, 62060L (2006).

[48] S. Iyer, L. Wu, J. Li, S. Potoczny, K. Matney, and P. R. C. Kent, J. Appl. Phys. **101**, 113508 (2007).

[49] A. Lindsay, E. P. O'Reilly, A. D. Andreev, and T. Ashley, Phys. Rev. B **77**, 165205 (2008).

[50] V. Virkkala, V. Havu, F. Tuomisto, and M. J. Puska, Phys. Rev. B **85**, 085134 (2012).

[51] J. J. Mudd, N. J. Kybert, W. M. Linhart, L. Buckle, T. Ashley, P. D. C. King, T. S. Jones, M. J. Ashwin, and T. D. Veal, Appl. Phys. Lett. **103**, 042110 (2013).

[52] R. C. Newman, Adv. Phys. **18**, 545 (1969).

[53] *Semiconductors and Semimetals*, edited by M. Stavola (Academic, New York, 1999), Vol. 51B, Chap. 4.

[54] M. D. McCluskey, J. Appl. Phys. **87**, 3593 (2000).

[55] A. M. Mintairov, P. A. Blagnov, V. G. Melehin, N. N. Faleev, J. L. Merz, Y. Qiu, S. A. Nikishin, and H. Temkin, Phys. Rev. B **56**, 15836 (1997).

[56] T. Prokofyeva, T. Sauncy, M. Seon, M. Holtz, Y. Qiu, S. Nikishin, and H. Temkin, Appl. Phys. Lett. **73**, 1409 (1998).

[57] H. Ch. Alt, A. Yu. Egorov, H. Riechert, B. Wiedemann, J. D. Meyer, R. W. Michelmann, and K. Bethge, Appl. Phys. Lett. **77**, 3331 (2000).

[58] J. Wagner, T. Geppert, K. Köhler, P. Ganser, and N. Herres, J. Appl. Phys. **90**, 5027 (2001).

[59] A. Mascarenhas and M. J. Seong, Semicond. Sci. Technol. **17**, 823 (2002).

[60] H. C. Alt and Y. V. Gomeniuk, Phys. Rev. B **70**, 161314(R) (2004).

[61] M. Güngerich, P. J. Klar, W. Heimbrodt, J. Koch, W. Stolz, M. P. Halsall, and P. Harmer, Phys. Rev. B **71**, 075201 (2005).

[62] S. J. Barker, R. S. Williams, C. P. A. Mulcahy, M. J. Steer, M. Hopkinson, M. J. Ashwin, R. C. Newman, P. N. Stavrinou, G. Parry, and T. S. Jones, Thin Solid Films **515**, 4430 (2007).

[63] A. M. Teweldeberhan and S. Fahy, Phys. Rev. B **72**, 195203 (2005).

[64] A. M. Teweldeberhan and S. Fahy, Phys. Rev. B **73**, 245215 (2006).

[65] A. M. Teweldeberhan and S. Fahy, Phys. Rev. B **77**, 235216 (2008).

[66] J. Buckeridge, A. M. Teweldeberhan, and S. Fahy, Phys. Rev. B **79**, 153201 (2009).

[67] A. M. Teweldeberhan, G. Stenuit, S. Fahy, E. Gallardo, S. Lazić, J. M. Calleja, J. Miguel-Sánchez, M. Montes, A. Hierro, R. Gargallo-Caballero, A. Guzmán, and E. Muñoz, Phys. Rev. B **77**, 155208 (2008).

[68] J. Buckeridge, S. O'Halloran, and S. Fahy, Solid State Commun. **150**, 1967 (2010).

[69] M. J. Ashwin, R. J. H. Morris, D. Walker, P. A. Thomas, M. G. Dowsett, T. S. Jones, and T. D. Veal, J. Phys. D **46**, 264003 (2013).

[70] G. Kresse and J. Hafner, Phys. Rev. B **47**, 558 (1993).

[71] G. Kresse and J. Hafner, Phys. Rev. B **49**, 14251 (1994).

[72] G. Kresse and J. Furthmüller, Comput. Mater. Sci. **6**, 15 (1996).

[73] G. Kresse and J. Furthmüller, Phys. Rev. B **54**, 11169 (1996).

[74] J. P. Perdew, K. Burke, and M. Ernzerhof, Phys. Rev. Lett. **77**, 3865 (1996).

[75] J. P. Perdew, A. Ruzsinszky, G. I. Csonka, O. A. Vydrov, G. E. Scuseria, L. A. Constantin, X. Zhou, and K. Burke, Phys. Rev. Lett. **100**, 136406 (2008).

[76] P. E. Blöchl, Phys. Rev. B **50**, 17953 (1994).

[77] T. C. Chiang and D. E. Eastman, Phys. Rev. B **22**, 2940 (1980).

[78] P. S. Dutta, H. L. Bhat, and V. Kumar, J. Appl. Phys. **81**, 5821 (1997).

[79] H. J. Monkhorst and J. D. Pack, Phys. Rev. B **13**, 5188 (1976).

[80] A. Togo, F. Oba, and I. Tanaka, Phys. Rev. B **78**, 134106 (2008).

[81] R. M. Pick, M. H. Cohen, and R. M. Martin, Phys. Rev. B **1**, 910 (1970).

[82] P. Giannozzi, S. de Gironcoli, P. Pavone, and S. Baroni, Phys. Rev. B **43**, 7231 (1991).

[83] X. Gonze and C. Lee, Phys. Rev. B **55**, 10355 (1997).

[84] D. E. Aspnes and A. A. Studna, Phys. Rev. B **27**, 985 (1983).

[85] I. V. Skryabinskii and Y. I. Ukhanov, Sov. Phys. Solid State **14**, 2838 (1973).

[86] C. G. Van de Walle and J. Neugebauer, J. Appl. Phys. **95**, 3851 (2004).

[87] C. Persson, Y.-J. Zhao, S. Lany, and A. Zunger, Phys. Rev. B **72**, 035211 (2005).

[88] N. N. Sirota and F. M. Gololobov, Dokl. Akad. Nauk SSSR **144**, 398 (1962).

[89] H. J. McSkimin, A. Jayaraman, J. P. Andreatch, and T. B. Bateman, J. Appl. Phys. **39**, 4127 (1968).

[90] W. F. Boyle and R. J. Sladek, Phys. Rev. B **11**, 2933 (1975).

[91] S.-H. Wei, L. G. Ferreira, and A. Zunger, Phys. Rev. B **41**, 8240 (1990).

[92] S. B. Zhang and M. L. Cohen, Phys. Rev. B **35**, 7604 (1987).

[93] B. K. Agrawal, P. S. Yadav, S. Kumar, and S. Agrawal, Phys. Rev. B **52**, 4896 (1995).

[94] S. Q. Wang and H. Q. Ye, Phys. Status Solidi B **240**, 45 (2003).

[95] J. Tan, Y. Li, and G. Ji, Comp. Mater. Sci. **58**, 243 (2012).

[96] K. Aoki, E. Anastassakis, and M. Cardona, Phys. Rev. B **30**, 681 (1984).

[97] T. C. McGlinn, T. N. Krabach, M. V. Klein, G. Bajor, J. E. Greene, B. Kramer, S. A. Barnett, A. Lastras, and S. Gorbatkin, Phys. Rev. B **33**, 8396 (1986).

[98] P. B. Klein and R. K. Chang, Phys. Rev. B **14**, 2498 (1976).

[99] M. K. Farr, J. G. Traylor, and S. K. Sinha, Phys. Rev. B **11**, 1587 (1975).

[100] S. Shinde, M. Talati, P. Jha, and S. Sanyal, Pramana **63**, 425 (2004).

[101] D. Berdekas, J. Eng. Sci. Tech. Rev. **2**, 24 (2009).

[102] Our formation energy calculations are performed under the assumption of thermodynamic equilibrium. The growth of $GaSb_{1-x}N_x$ is a nonequilibrium process, meaning kinetics may dominate the defect chemistry. It is possible, therefore, that $(N-Sb)_{Sb}$, which has a relatively lower formation energy in comparison with the other N interstitial configurations, occurs in significant quantities. By calculating its associated vibrational frequencies, we predict an experimental signature for this defect.

[103] *CRC Handbook of Chemistry and Physics*, 89th ed., edited by D. R. Lide (CRC, Boca Raton, FL, 2008).

[104] D. O. Scanlon, P. D. C. King, R. P. Singh, A. de la Torre, S. McKeown Walker, G. Balakrishnan, F. Baumberger, and C. R. A. Catlow, Adv. Mater. **24**, 2154 (2012).

[105] S. Chen, X. G. Gong, A. Walsh, and S.-H. Wei, Appl. Phys. Lett. **94**, 041903 (2009).

[106] A. A. Sokol, S. A. French, S. T. Bromley, C. R. A. Catlow, H. J. J. van Dam, and P. Sherwood, Faraday Discuss. **134**, 267 (2007).

[107] S. J. Clark, J. Robertson, S. Lany, and A. Zunger, Phys. Rev. B **81**, 115311 (2010).

[108] M. Burbano, D. O. Scanlon, and G. W. Watson, J. Am. Chem. Soc. **133**, 15065 (2011).

[109] D. O. Scanlon and G. W. Watson, J. Mater. Chem. **21**, 3655 (2011).

[110] D. O. Scanlon, Phys. Rev. B **87**, 161201 (2013).

[111] P. Carrier, S.-H. Wei, S. B. Zhang, and S. Kurtz, Phys. Rev. B **71**, 165212 (2005).

[112] S. B. Zhang and S.-H. Wei, Phys. Rev. Lett. **86**, 1789 (2001).

[113] W. M. Theis, K. K. Bajaj, C. W. Litton, and W. G. Spitzer, Appl. Phys. Lett. **41**, 70 (1982).

[114] X. K. Chen, R. Wiersma, C. X. Wang, O. J. Pitts, C. Dale, C. R. Bolognesi, and S. P. Watkins, Appl. Phys. Lett. **80**, 1942 (2002).